Bergische Universität Wuppertal

Fakultät für Mathematik und Naturwissenschaften

Institute of Mathematical Modelling, Analysis and Computational Mathematics (IMACM)

Preprint BUW-IMACM 23/13

Sergey Pereselkov, Venedikt Kuz'kin, Matthias Ehrhardt, Sergey Tkachenko, Pavel Rybyanets and Nikolay Ladykin

3D Modeling of Sound Field Hologram of Moving Source in Presence of Internal Waves Causing Horizontal Refraction

August 23, 2023

http://www.imacm.uni-wuppertal.de

Article

3D Modeling of Sound Field Hologram of Moving Source in Presence of Internal Waves Causing Horizontal Refraction

Sergey Pereselkov [1,*], Venedikt Kuz'kin [2], Matthias Ehrhardt [3], Sergey Tkachenko [1], Pavel Rybyanets [1] and Nikolay Ladykin [1]

[1] Voronezh State University, Mathematical Physics and Information Technology Department , 394018 Voronezh, Russia; tkachenko.edu@yandex.ru (S.T.); rybyanets.edu@yandex.ru (P.R.); ladykin.edu@yandex.ru (N.L.)
[2] Prokhorov General Physics Institute of the Russian Academy of Sciences, 119991, Moscow, Russia ; kumiov@yandex.ru
[3] University of Wuppertal, Chair of Applied and Computational Mathematics, Gaußstraße 20, 42119 Wuppertal, Germany; ehrhardt@uni-wuppertal.de
* Correspondence: pereselkov@yandex.ru

Abstract: In this paper we study the variations of the sound field hologram of a moving source in an inhomogeneous ocean waveguide. It is assumed that intense internal waves (internal solitons) are the reason for the inhomogeneities of the shallow water waveguide. The results of 3D modeling of the sound field considering horizontal refraction by internal waves are presented. In the context of 3D modeling, the interferogram (sound intensity distributions in the frequency-time domain) and the hologram (2D Fourier transform of the interferogram) of moving sources are analyzed. The hologram of the moving source consists of two disjoint regions corresponding to the unperturbed field and the field perturbed by internal waves. This structure of the hologram allows the reconstruction of the interferogram of the unperturbed field in a shallow water waveguide in the absence of intense internal waves. The error in the reconstruction of the unperturbed interferogram is estimated.

Keywords: shallow water; sound field; modes interference; interferogram; hologram; internal waves

check for updates

Citation: Pereselkov, S.; Kuz'kin, V.; Ehrhardt, M.; Tkachenko, S.; Rybyanets, P.; Ladykin, N. 3D Modeling of Sound Field Hologram of Moving Source in Presence of Internal Waves Causing Horizontal Refraction. *Preprints* **2023**, *1*, 0. https://doi.org/

Academic Editor:

Copyright: © 2023 by the authors. Licensee MDPI, Basel, Switzerland. This article is an open access article distributed under the terms and conditions of the Creative Commons Attribution (CC BY) license (https://creativecommons.org/licenses/by/4.0/).

1. Introduction

Currently, there is a great scientific interest in interferometric signal processing in underwater acoustics. The interferometric signal processing based on stable structural features of the interference pattern of the broadband sound field in shallow water waveguide. We refer the interested reader to the most relevant papers [1–12] in which significant results have been obtained in this direction for regular waveguides without inhomogeneities.

The holographic signal processing [13–22] is one of the most advantageous approaches of interferometric methods. In holographic processing [15,16], a quasi-coherent accumulation of spectral density along localized fringes of an interference pattern (interferogram $I(\omega, t)$) is performed in frequency-time variables [13,14]. An interferogram $I(\omega, t)$ is understood as the square of the modulus of the received signal in frequency-time variables. The geometry of the localized bands is determined by the parameters of the waveguide and source parameters (range, velocity, movement direction) [15,16]. A two-dimensional Fourier transform (2D-FT) is applied to the accumulated spectral density of the interferogram $I(\omega, t)$ [13–17]. The result of the 2D-FT of the interferogram $I(\omega, t)$ is called Fourier-hologram (hologram $F(\tau, \widetilde{\nu})$). The hologram $F(\tau, \widetilde{\nu})$ is localized in a narrow band as focal spots corresponding to the interference of different modes.

The physical and mathematical principles of hologram formation were first described in [13,14]. In the development of holographic processing [13–22], it was assumed that the oceanic environment is homogeneous, i.e., that its parameters are constant in the space-time domain.

However, in many cases, acoustic signals propagate in waveguides with hydrodynamic perturbations. The hydrodynamic perturbations of the waveguide leads to a distortion of the interferogram $I(\omega, t)$ and an increase of the focal spots in the hologram $F(\tau, \widetilde{\nu})$. In the presence of hydrodynamic perturbations, the interferogram can be presented

as the sum of two components. The first of them corresponds waveguide in absence of the perturbation and the second one is due to waveguide perturbation. Since the 2D-FT is a linear transform, the hologram $F(\tau, \widetilde{\nu})$ can be represented as a superposition of two hologram-components. These components consist of a hologram component related to the source in the unperturbed waveguide and a hologram component due to waveguide perturbation.

In inhomogeneous waveguides, the holographic signal processing was first considered for experimental data processing obtained in the SWARM-95 experiment [23–26]. It was shown that holographic signal processing allows to separate the interferogram components of the unperturbed and perturbed sound fields [27,28]. This experimental result was described theoretically and verified by numerical modeling in the papers [29,30]. The aim of this work is to present the results of numerical modeling of holographic signal processing for a moving source and a non-moving receiver in the presence of *intense internal waves* (IIWs) causing significant horizontal refraction. The IIWs influence on the error of the source parameters estimations (range, velocity and movement direction) are analysed.

The paper consists of five sections. After the introduction in Section 1 we describe in Section 2 the 3D model of a shallow water waveguide in the presence of IIWs. Next, in Section 3, we derive the mathematical models of the interferogram $I(\omega, t)$ and the hologram $F(\tau, \widetilde{\nu})$ of a moving source in a shallow water waveguide in presence of the IIWs. The algorithm of the numerical calculation of the interferogram and hologram of moving source is developed. It is based on vertical modes and the horizontal parabolic approximation approach. The proposed algorithm allows to take into account the horizontal refraction of the sound field caused by IIWs propagating across the acoustic track (source-receiver). The results of the numerical modeling of the interferogram $I(\omega, t)$ and hologram $F(\tau, \widetilde{\nu})$ of the broadband sound source in the shallow water waveguide in the presence of IIWs causing horizontal refraction are analyzed in Section 4. Within the numerical modeling, the influence of IIWs on the interferogram $I(\omega, t)$ and hologram $F(\tau, \widetilde{\nu})$ of the source sound field is considered for two different cases of source parameters. The first case is a stationary acoustic track source-receiver (non-moving source). The second case is a non-stationary acoustic trace (moving source). In order to compare the numerical modeling results for both cases in the presence of IIWs, the initial data for the simulation are chosen to be the same. The IIWs influence on the error of the source parameters estimates (range, velocity) are analysed.

2. Shallow Water Waveguide Model in Presence of Internal Waves

In this section, we describe the 3D model of the shallow water waveguide used in our research (Figure 1). The shallow water waveguide in the Cartesian coordinate system (X, Y, Z) is represented as a water layer with a sound velocity $c(x, y, z, t)$ and a density $\rho(x, y, z, t)$. The water layer is confined in depth by a free surface $(z = 0)$ and a homogeneous absorbing half-space $(z = H)$ - the sea bottom.

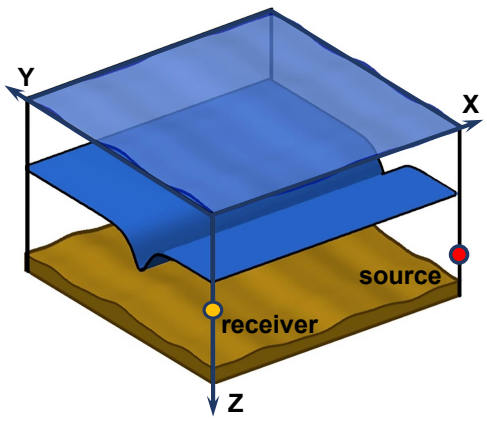

Figure 1. Shallow water model in presence of internal waves.

The complex refractive index and density of the bottom are denoted by $n_b(1+\mathrm{i}\varkappa)$, ρ_b [31]. The parameter $\varkappa = \chi c_b/54.6f$ is determined by the bottom loss coefficient - χ, the bottom sound speed - c_b and the sound frequency - f. The space-time of the sound speed in the water layer can be represented in the following form:

$$c(x,y,z,t) = c(z) + \delta c(x,y,z,t), \tag{1}$$

with $c(z)$ - sound speed profile in the waveguide in the absence of the IIWs, $\delta c(x,y,z,t)$ - sound speed variations caused by the IIWs. According to Eq. (1), the squared refractive index in the water layer is

$$n^2(x,y,z_q,t) = \bar{n}^2(z) + \tilde{n}^2(x,y,z,t), \tag{2}$$

where $\bar{n}^2(z)$ corresponds to the unperturbed waveguide, $\tilde{n}^2(x,y,z,t)$ is due to IIWs.

According to [32,33] we have

$$\tilde{n}^2(x,y,z,t) = -2QN^2(z)\,\zeta(x,y,z,t). \tag{3}$$

Here, $Q \approx 2.4$ s^2/m is a constant determined by the water physical properties; $N(z) = (g\rho^{-1}d\rho/dz)^{1/2}$ is the buoyancy frequency, $\zeta(x,y,z,t)$ are the vertical displacements in the water layer due to IIWs. According to the predominance of the first gravitational mode [34], $\zeta(x,y,z,t)$ can be written as follows

$$\zeta(x,y,z,t) = \Phi_1(z)\,\zeta_0(x,y,t), \tag{4}$$

where $\Phi_1(z)$ denotes the eigenfunction of the first gravity mode, normalized at depth z_0: $\Phi_1(z_0) = 1$; $\zeta_0(x,y,t)$ are vertical displacements in waveguide water layer due to IIWs at depth z_0.

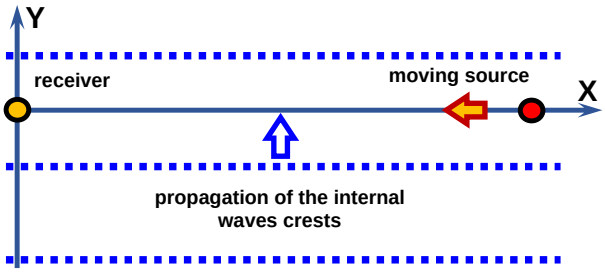

Figure 2. Problem geometry. Acoustic track (source-receiver) orientation relative to IIWs.

According to [34] we can represent IIWs as the sequence of internal solitons (IS - soliton-like solution of KdV-equation). Given the chosen problem geometry (Figure 2), the vertical displacements in the water layer of the waveguide $\zeta_0(x,y,t)$ can be described as

$$\zeta_0(x,y,t) = \sum_{n=1}^{N} -B_n \operatorname{sech}^2\left[(y - D_n - u_n t)/\eta_n\right], \tag{5}$$

where N - count of the IS in train, B_n - IS amplitude, u_n - IS velocity, D_n - IS shift in horizontal plane, η_n - IS width.

IIWs - hydrodynamic phenomenon, which is widespread in the oceanic environment. In shallow waters they are trains of intense short-period vertical displacements in the water layer of the ocean waveguide. They are described as trains of IS that propagate to the shelf coast. The reason for the IIWs are internal tides [34]. According to experimental data [34], the parameters of IIWs are the following:
- train length: $\sim 3-5$ km ($N \sim 4-7$);
- ζ has quasi-sinusoidality form (narrow spatial spectrum);
- ζ are synchronized in depth (dominance of the $\Phi_1(z)$);

- propagation velocity: $u_n \sim 0.5 - 1\,\mathrm{m/s}$;
- IS amplitude: $B_n \sim 10 - 30\,\mathrm{m}$;
- IS width: $\eta_n \sim 100 - 200\,\mathrm{m}$;
- interval between IS: $\sim 300 - 500\,\mathrm{m}$;
- curvature radius of IS front in horizontal plane $\sim 15 - 25\,\mathrm{km}$.

These parameters lead to specific acoustic phenomena due to IIWs. In [32,33] it is shown that the presence of IIWs causes significant horizontal refraction of sound rays, which is at a small angle to the wavefront of the IIWs. As a result, the dynamic waveguides are approximately parallel to the IIWs fronts in the horizontal plane. Within the "vertical modes and horizontal rays" approach, it is shown that horizontal dynamic waveguides have selective character for sound modes. The structure of horizontal rays is different for different sound modes. It is shown that the structure of horizontal rays of sound modes also depends on frequency [32,33]. This frequency dependence of horizontal refraction has a resonance-like form and is evident in the propagation of broadband sound signals.

3. Interferogram and Hologram of Moving Source

In the framework of the "vertical modes and horizontal parabolic approximation" approach, the complex sound field in the shallow-water waveguide in the presence of the IIWs equations (1)–(5) can be written in the following way [32,33]:

$$p(\mathbf{r}, z, \omega, t) = \sum_{m=0}^{M} P_m(\mathbf{r}, \omega, t)\, \phi_m(z, \omega) \exp\left[\mathrm{i}(\bar{h}_m + \mathrm{i}\bar{\gamma}_m)x\right], \tag{6}$$

where $\mathbf{r} = (x, y)$ is the radius vector of the source in the horizontal plane, P_m is the mode amplitude, $\bar{h}_m + \mathrm{i}\bar{\gamma}_m$ is the complex horizontal wavenumber of the m-th acoustic mode, where $\phi_m(z, \omega)$ is the corresponding acoustic mode in the waveguide without IIWs. In Eq.(6), summation is performed up to M, the total number of acoustic modes to be considered. Consequently, the acoustic pressure depends on the acoustic frequency $\omega = 2\pi f$.

The $\phi_m(\mathbf{r}, \omega, t)$ are the eigenfunctions (acoustic modes) and $h_m(\mathbf{r}, \omega, t)$ and $\gamma_m(\mathbf{r}, \omega, t)$ are the real and imaginary parts of the eigenvalues (horizontal wavenumbers) $\xi_m(\omega) = h_m(\mathbf{r}, \omega, t) + \mathrm{i}\gamma_m(\mathbf{r}, \omega, t)$, obtained by solving the Sturm-Liouville problem under the usual boundary conditions for free surface and bottom [31]. The horizontal wavenumber $h_m(x, z, t)$ of the m-th acoustic mode in a waveguide with IIWs can be represented as the sum of the unperturbed component ($\bar{h}_m(\omega)$) and the perturbation $\tilde{h}_m(\mathbf{r}, \omega, t)$ due to IIWs:

$$h_m(\mathbf{r}, \omega, t) = \bar{h}_m(\omega) + \tilde{h}_m(\mathbf{r}, \omega, t). \tag{7}$$

The linear correction in the framework of the perturbation theory [32,33] is determined by the expression

$$\tilde{h}_m(\mathbf{r}, \omega, t) = \frac{k^2}{2\bar{h}_m} \int_0^H \phi_m^2(z, \omega)\, \tilde{n}^2(\mathbf{r}, z, \omega, t)\, dz. \tag{8}$$

Here $k = \omega/c_0$ is the sound wavenumber, c_0 is the sound speed at depth z_0. Considering Eq. (3), we obtain for $\tilde{h}_m(\mathbf{r}, \omega, t)$ the expression:

$$\tilde{h}_m(\mathbf{r}, \omega, t) = -q_m(\omega)\zeta(\mathbf{r}, t), \tag{9}$$

where the coefficient $q_m(\omega)$ is given by

$$q_m(\omega) = \frac{Qk^2}{\bar{h}_m} \int_0^H \phi_m^2(z)\, N^2(z)\, \Phi_1(z)\, dz. \tag{10}$$

From Eq. (10) it follows that the horizontal structures depend on the acoustic mode numbers and on the frequency [32,33]. It also follows from Eq. (10) that the frequency dependence

of horizontal refraction has a resonance-like form and manifests itself in the propagation of broadband acoustic signals.

The mode amplitude $P_m(\mathbf{r},\omega,t)$ is determined as the solution of the parabolic equation:

$$\frac{\partial P_m}{\partial x} = \frac{\mathrm{i}}{2\bar{h}_m}\frac{\partial^2 P_m}{\partial y^2} + \frac{\mathrm{i}\bar{h}_m}{2}\left(n_m^2(\mathbf{r},\omega,t)-1\right)P_m, \tag{11}$$

where $n_m(\mathbf{r},\omega,t)$ - horizontal refractive index of the m-th acoustic mode in waveguide in presence of the IIWs:

$$n_m(\mathbf{r},\omega,t) = h_m(\mathbf{r},\omega,t)/\bar{h}_m. \tag{12}$$

The numerical solution of Eq. (12) is performed using the "Split Step Fourier" (SSF) algorithm [35,36]:

$$\begin{aligned} &P_m(x+\Delta x,y,\omega,t)\\ &= \exp\left[-\mathrm{i}\bar{h}_m\Delta x U_m(x,y,\omega,t)\right]\times \mathrm{FFT}^{-1}\left\{\exp\left[\mathrm{i}\bar{h}_m\Delta x T_m(h)\right]\times \mathrm{FFT}\left[P_m^*(x,y,\omega,t)\right]^*\right\}. \end{aligned} \tag{13}$$

Here FFT - forward Fast Fourier Transformation operator, FFT^{-1} - backward Fast Fourier Transformation operator, $T_m(h) = 0.5(h/\bar{h}_m)^2$ - operator in the Fourier Space of wavenumbers $\bar{h}_m$, $U_m(x,y,\omega,t) = -0.5\left(n_m^2(x,y,\omega,t)-1\right)$ - operator in the space of coordinates (x,y) in the horizontal plane.

In the framework of the "vertical modes and horizontal parabolic approximation" (Eq. (6)), the interference pattern of the sound intensity distribution $I(\omega,t)$ of the moving source - (interferogram) in the frequency-time domain (ω,t) can be written as:

$$\begin{aligned} I(\omega,t) &= \sum_m\sum_n P_m(\omega,t)\,P_n^*(\omega,t)\exp\left[\mathrm{i}\bar{h}_{mn}(\omega)(x_0-vt)\right]\\ &= \sum_m\sum_n I_{mn}(\omega,t), \quad m\neq n, \end{aligned} \tag{14}$$

where $\bar{h}_{mn}(\omega) = \bar{h}_m(\omega) - \bar{h}_n(\omega)$. Here, $I_{mn}(\omega,t)$ - partial interferogram produced by interference of m-th and n-th modes, $P_m(\omega,t)$ - amplitude of the $m-$th acoustic mode, x_0 - initial source coordinate at time $t_0 = 0$, t - current time, v - velocity of the moving source. The superscript "*" denotes the complex conjugate value. The mode attenuation, and depths of the source z_s and receiver z_q are taken into account by the mode amplitude $P_m(\omega,t)$. The condition $m \neq n$ means that the mean value has been removed from the interferogram $I(\omega,t)$.

Let us consider a hologram of the moving sound source in the presence of the IIWs. We apply a 2D-dimensional Fourier transform (2D-FT) to the interferogram $I(\omega,t)$ (Eq. (14)) in the frequency-time variables (ω,t). The result of the 2D-FT is called Fourier hologram (hologram) $F(\tau,\tilde{\nu})$:

$$\begin{aligned} F(\tau,\tilde{\nu}) &= \sum_m\sum_n \int_0^{\Delta t}\int_{\omega_1}^{\omega_2} I_{mn}(\omega,t)\exp\left[\mathrm{i}(\tilde{\nu}t-\omega\tau)\right]dt\,d\omega\\ &= \sum_m\sum_n F_{mn}(\tau,\tilde{\nu}), \end{aligned} \tag{15}$$

where τ and $\tilde{\nu} = 2\pi\nu$ are the time and circular frequency in the hologram domain, $F_{mn}(\tau,\tilde{\nu})$ - partial hologram produced by interference of m-th and n-th modes, $\omega_1 = \omega_0 - (\Delta\omega/2)$, $\omega_2 = \omega_0 + (\Delta\omega/2)$ - integral limits, $\Delta\omega$ - frequency band, ω_0 - reference frequency, Δt - observation time.

We consider the linear approximation of the waveguide dispersion:

$$\bar{h}_m(\omega) = \bar{h}_m(\omega_0) + \frac{\mathrm{d}\bar{h}_m(\omega_0)}{\mathrm{d}\omega}(\omega-\omega_0). \tag{16}$$

It is assumed that sound field spectrum and mode amplitude P_m as a function of frequency ω are slow compared to the fast oscillation of $\exp[\mathrm{i}h_m(\omega)(x_0+vt)]$. Under this assumption, the partial hologram equation Eq. (15) reads:

$$F_{mn}(\tau,\widetilde{\nu}) = P_m(\omega_0)P_n^*(\omega_0)\Delta\omega\Delta t\exp[\mathrm{i}\Phi_{mn}(\tau,\widetilde{\nu})]\times \\ \times\frac{\sin\Big\{\big[x_0\frac{\mathrm{d}h_{mn}(\omega_0)}{\mathrm{d}\omega}-\tau\big]\frac{\Delta\omega}{2}\Big\}\sin\Big\{\big[vh_{mn}(\omega_0)+\widetilde{\nu}\big]\frac{\Delta t}{2}\Big\}}{\big[x_0\frac{\mathrm{d}h_{mn}(\omega_0)}{\mathrm{d}\omega}-\tau\big]\frac{\Delta\omega}{2}\big[vh_{mn}(\omega_0)+\widetilde{\nu}\big]\frac{\Delta t}{2}}, \quad (17)$$

where $\Phi_{mn}(\tau,\widetilde{\nu})$ is the phase of the $F_{mn}(\tau,\widetilde{\nu})$ - partial hologram produced by interference of m-th and n-th modes.

$$\Phi_{mn}(\tau,\widetilde{\nu}) = \Big(\frac{\widetilde{\nu}\Delta t}{2}-\tau\omega_0\Big)+h_{mn}(\omega_0)\Big(\frac{\Delta t}{2}v+x_0\Big). \quad (18)$$

In Eq. (17) the approximation $x_0 \gg v\Delta t$ is used.

The hologram distribution $F(\tau,\tilde{\nu})$ in domain $(\tau,\tilde{\nu})$ is localized in two narrow areas as focal spots. They are located:

1. in I and III quadrants, when source moves to receiver ($v<0$);
2. in II and IV quadrants, when source moves away from receiver, ($v>0$).

The hologram distribution $F(\tau,\tilde{\nu})$ contains $(M-1)$ focal spots with coordinates $(\tau_\mu,\widetilde{\nu}_\mu)$ lying on the straight line $\widetilde{\nu}=\widetilde{\varepsilon}\tau$. Here, $\mu=\overline{1,M-1}$ is the number of the focal spot. In the focal spot with coordinates $(\tau_\mu,\widetilde{\nu}_\mu)$ the maxima of $(M-\mu)$ partial holograms accumulate.

The angular coefficient $\widetilde{\varepsilon}=2\pi\varepsilon$ can be represented in the form $\widetilde{\varepsilon}=-\delta\omega/\delta t$, where $\delta\omega$ is the frequency shift of the interference maximum during the observation time δt. The dimensions of the focal spots $\delta\tau$, $\delta\widetilde{\nu}$ along τ, $\widetilde{\nu}$ do not depend on the number of focal spots and are the same: $\delta\tau=4\pi/\delta\omega$, $\delta\widetilde{\nu}=4\pi/\delta t$.

For the first focal spot closest to the origin, the radial velocity and initial distance are given as [**?**]:

$$\dot{v}=-k_v\widetilde{\nu}_1, \qquad \dot{x}_0=k_x\tau_1, \quad (19)$$

where

$$k_v=(M-1)\Big(h_{1M}(\omega_0)\Big)^{-1}, \qquad k_x=(M-1)\Big(\mathrm{d}h_{1M}(\omega_0)/\mathrm{d}\omega\Big)^{-1}. \quad (20)$$

In contrast to the true values, the estimated source parameters are marked by a dot at the top. The holographic method of signal processing is realized in the following way. During the observation time Δt, in the frequency band $\Delta\omega$ J independent signal realizations of duration t_1 with a time interval t_2 are quasi-coherently accumulated along the interference fringes:

$$J=\Delta t/(t_1+t_2). \quad (21)$$

Signal realizations are independent if $t_2>2\pi/\Delta\omega$. In this way, the interferogram $I(\omega,t)$ is formed and the 2D FT transform is applied to it. As result, the hologram $F(\tau,\widetilde{\nu})$ of the moving source in the shallow water waveguide is obtained.

In general, the structures of the interferogram $I(\omega,t)$ and the hologram $F(\tau,\widetilde{\nu})$ are very different. However, a hologram $F(\tau,\widetilde{\nu})$ is a unique representation of an interferogram $I(\omega,t)$. Thus, the inversion of the hologram $F(\tau,\widetilde{\nu})$ (using the inverse 2D-FT transform) allows the reconstruction of the original interferogram $I(\omega,t)$.

4. Results of Numerical Simulation

The results of numerical modeling of the interferogram $I(\omega,t)$ and hologram $F(\tau,\widetilde{\nu})$ of the broadband sound source in the shallow water waveguide in the presence of IIWs causing horizontal refraction are analyzed in Section 4. Within the numerical modeling, the influence of IIWs on the interferogram and hologram of the source sound field is considered

for two different cases of source parameters. The first case is a stationary acoustic track source-receiver (non-moving source). The second case is a non-stationary acoustic trace (moving source). In order to compare the numerical modeling results for both cases in the presence of IIWs, the initial data for the simulation are chosen to be the same.

Section 4 consists of three parts. The shallow water waveguide and source parameters are described in Section 4.1. The numerical modeling results for stationary acoustic trace source-receiver (non-moving source) are presented in Section 4.2. The numerical modeling results for non-stationary acoustic track source-receivers (moving source) are analyzed in Section 4.3.

4.1. Waveguide parameters

Consider a shallow water waveguide with parameters related to the SWARM'95 (1995) experiment on the New Jersey coast [15]. The sound speed profile $c(z)$ in the water layer of the waveguide is shown in Figure 3.

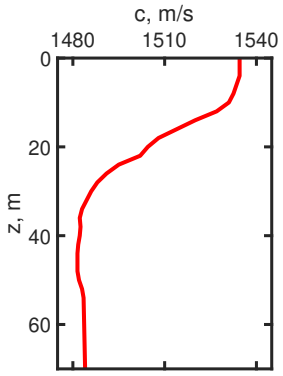

Figure 3. Sound speed profile $c(z)$. Experiment SWARM'95 (1995) [15].

In the context of numerical modeling, the following two frequency ranges are considered:

1. $\Delta f_1 = 100 - 120\,\text{Hz}$;
   Bottom refractive index $n_b = 0.84\,(1 + \text{i}\,0.03)$;
   Bottom density $\rho_b = 1.8\,\text{g/cm}^3$;
   Modes count $M = 4$.
2. $\Delta f_2 = 300 - 320\,\text{Hz}$;
   Bottom refractive index $n_b = 0.84\,(1 + \text{i}\,0.05)$;
   Bottom density $\rho_b = 1.8\,\text{g/cm}^3$;
   Modes count $M = 10$.

The wavenumbers of the modes $h_m(\omega_0)$ and their derivatives $dh_m(\omega_0)/d\omega$ at mid-range frequencies are given in Table 1 ($f_{01} = 110\,\text{Hz}$) and Table 2 ($f_{02} = 310\,\text{Hz}$).

Table 1. Modes parameters. Frequency $f_{01} = 110\,\text{Hz}$

Mode numbers, m	**1**	**2**	**3**	**4**
h_m, m^{-1}	0.4635	0.4557	0.4450	0.4310
$(dh_m/d\omega)10^4, (\text{m/s})^{-1}$	6.7624	6.8085	6.9014	7.0914

Table 2. Modes parameters. Frequency $f_{02} = 310\,\text{Hz}$

Mode numbers, m	**1**	**2**	**3**	**4**	**5**	**6**	**7**	**8**	**9**	**10**
h_m, m^{-1}	1.3123	1.3073	1.3006	1.2920	1.2826	1.2730	1.2630	1.2525	1.2403	1.2258
$(dh_m/d\omega)10^4, (\text{m/s})^{-1}$	6.7511	6.7619	6.7813	6.7973	6.8080	6.8150	6.8312	6.8753	6.9703	7.0574

The problem geometry: acoustic track (source-receiver), IIWs propagation direction, source motion direction are shown in Figure 2. An IIWs train Eq. (5) consists of three identical IS ($N = 3$). The IS parameters are as follows:
- amplitude $B_n = 20\,\text{m}$;
- width $\eta_n = 200\,\text{m}$;
- velocity $u_n = 0.7\,\text{m/s}$;
- distance between IS $\Lambda = 500\,\text{m}$;
- straight wavefront in horizontal plane.

4.2. Non-moving source ($v = 0$ m/s)

Let us consider the results of numerical modeling for a non-moving source ($v = 0\,\text{m/s}$). The source-receiver range $x_0 = 10\,\text{km}$. The source depth is $z_s = 20\,\text{m}$. The receiver depth $z_q = 45\,\text{m}$. The source spectrum is uniform. The sound pulses are recorded periodicity with interval 5s. The sampling frequency is 0.25 Hz. The observation time is $T = 20\,\text{min}$. The two frequency bands $\Delta f_1 = 100 - 120\,\text{Hz}$ (Table 1) and $\Delta f_2 = 300 - 320\,\text{Hz}$ (Table 2) are considered.

The results of the numerical modeling are shown in Figures 4–11. Figures 4 and 5 show the interferogram $I(f,t)$ and the hologram $F(\tau,\widetilde{\nu})$ for the case of the absence of IIWs. Figure 4 corresponds to $\Delta f_1 = 100 - 120\,\text{Hz}$ and Figure 5 to $\Delta f_2 = 300 - 320\,\text{Hz}$. The interferograms $I(f,t)$ consist of localized vertical fringes. The hologram $F(\tau,\widetilde{\nu})$ consists of focal spots on the horizontal axis. This is the result of a non-moving source. The irregularity of the interferogram $I(f,t)$ and the number of focal spots in the hologram $F(\tau,\widetilde{\nu})$ increase with frequency. This is explained by the increase in the number of acoustic modes in the sound field.

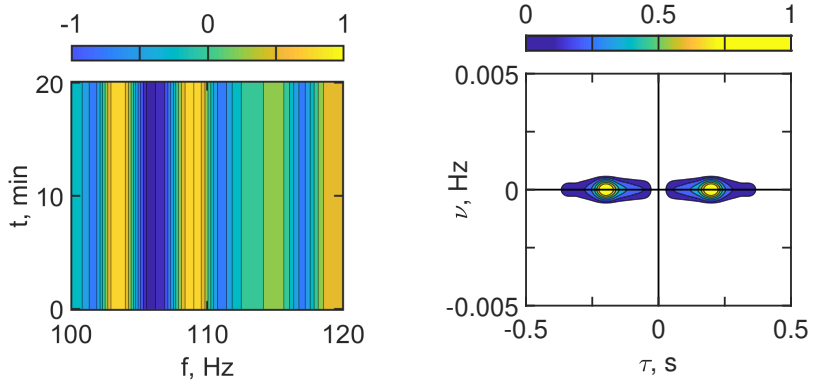

Figure 4. Normalized interferogram $I(f,t)$ (**a**) and hologram $F(\tau,\widetilde{\nu})$ (**b**). Frequency range $\Delta f_1 = 100 - 120\,\text{Hz}$. Non-moving source ($v = 0\,\text{m/s}$). IIWs are absent.

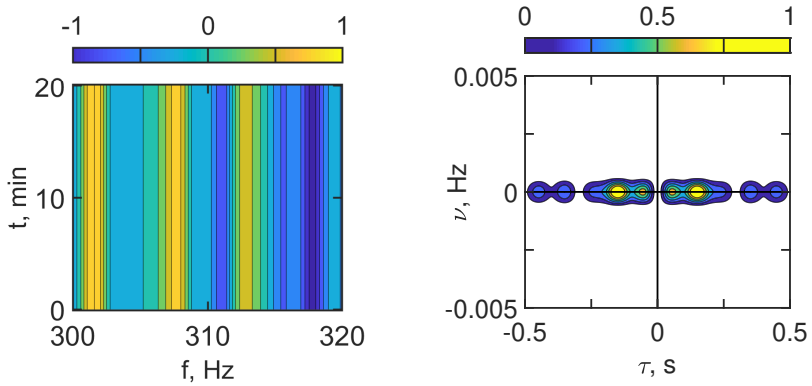

Figure 5. Normalized interferogram $I(f,t)$ (**a**) and hologram $F(\tau,\widetilde{\nu})$ (**b**). Frequency range $\Delta f_2 = 300-320$ Hz. Non-moving source ($v = 0$ m/s). IIWs are absent.

Figures 6 and 7 show the interferogram $I(f,t)$ and the hologram $F(\tau,\widetilde{\nu})$ in the case of IIWs presence. Figure 6 corresponds to $\Delta f_1 = 100-120$ Hz and Figure 7 to $\Delta f_2 = 300-320$ Hz. When the acoustic track is located between the IS crests (horizontal spatial period $\Lambda = 250$ m), the interferogram $I(f,t)$ contains horizontal fringes with the width $\Delta t = 5.9$ min. In this case, the sound field of the source is focused along the acoustic track due to the horizontal refraction caused by IIWs. Such structure of the interferogram $I(f,t)$ with horizontal fringes leads to the formation of a periodic structure of focal spots in the hologram $F(\tau,\widetilde{\nu})$.

The estimates for the focal spot sizes δf, δt, periodicity intervals L_f and L_t are as follows:

1. $\Delta f_1 = 100-120$ Hz;
   $\delta f_1 = 2.5$ Hz, $\delta t_1 = 1.3$ min;
   $L_{f_1} = 9.2$ Hz, $L_{t_1} = 8$ min.
2. $\Delta f_2 = 300-320$ Hz;
   $\delta f_2 = 3.5$ Hz, $\delta t_2 = 1.3$ min;
   $L_{f_2} = 5.5$ Hz, $L_{t_2} = 8$ min.

Under natural conditions, the IIWs train consists of different ISs with different parameters. This leads to a blurring of the pronounced periodic structure of interferogram $I(f,t)$ and hologram $F(\tau,\widetilde{\nu})$.

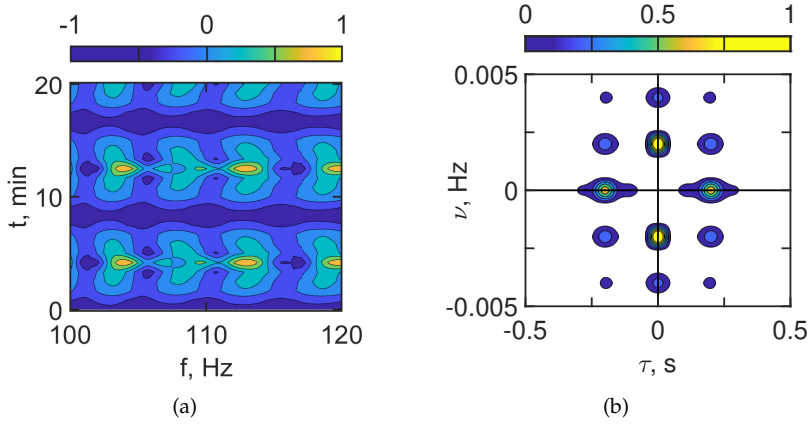

Figure 6. Normalized interferogram $I(f,t)$ (**a**) and hologram $F(\tau,\widetilde{\nu})$ (**b**). Frequency range $\Delta f_1 = 100-120$ Hz. Non-moving source ($v = 0$ m/s). IIWs are present ($B_n = 15$ m, $u_n = 0.7$ m/s).

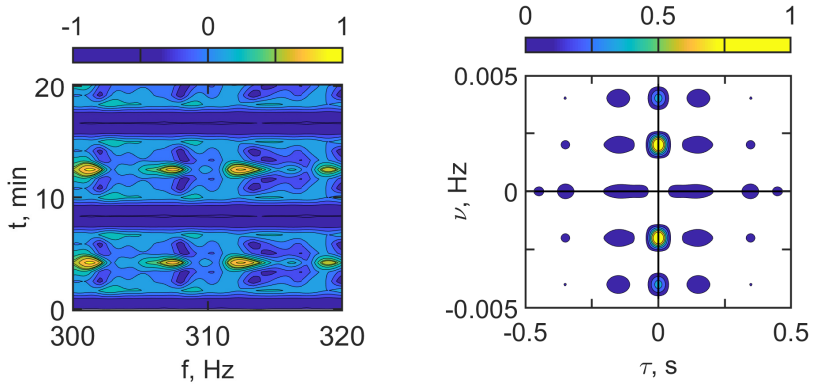

(a) (b)

Figure 7. Normalized interferogram $I(f,t)$ (**a**) and hologram $F(\tau,\widetilde{\nu})$ (**b**). Frequency range $\Delta f_2 = 300-320$ Hz. Non-moving source ($v = 0$ m/s). IIWs are present ($B_n = 15$ m, $u_n = 0.7$ m/s).

The structure of the focal spots arrangement in the hologram $F(\tau,\widetilde{\nu})$ allows the separation of the sound field component corresponding to the waveguide without IIWs and the sound field component related to the perturbation by IIWs.

The results of filtering the hologram focal spots located mainly on the horizontal axis in Figures 6 and 7 and their inverse 2D FT (interferogram) are shown in Figures 8 and 10. The reconstructed interferograms and holograms in Figures 8 and 10 correspond to the interferograms and holograms without IIWs in Figures 4 and 5. It can be seen that the focal spots on the reconstructed and the initial hologram are the same. The closeness of the initial and reconstructed interferograms is shown in Figure 11. Figure 11 shows the 1D interferograms for $t_0 = 0$min. Red curve - IIWs are absent. Blue curve - IIWs are present.

The error of the interferogram reconstruction is estimated by the dimensionless quantity:

$$d = \frac{\sum_{j=1}^{J} |I_1(f_j) - I_2(f_j)|}{\sum_{j=1}^{J} |I_1(f_j)|}, \tag{22}$$

where $I_1(f)$, $I_2(f)$ are initial and reconstructed 1D-interferograms, respectively.

1. $\Delta f_1 = 100-120$ Hz;
   $d_1 = 0.117$, $J = 80$.
2. $\Delta f_2 = 300-320$ Hz;
   $d_2 = 0.096$, $J = 80$.

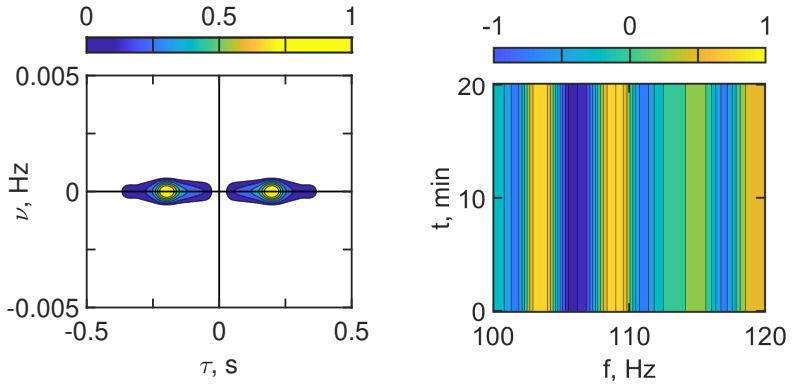

(a) (b)

Figure 8. Normalized filtered hologram $F(\tau,\widetilde{\nu})$ (**a**) and filtered interferogram $I(f,t)$ (**b**). Frequency range $\Delta f_1 = 100-120$ Hz. Non-moving source ($v = 0$ m/s). IIWs are present ($B_n = 15$ m, $u_n = 0.7$ m/s).

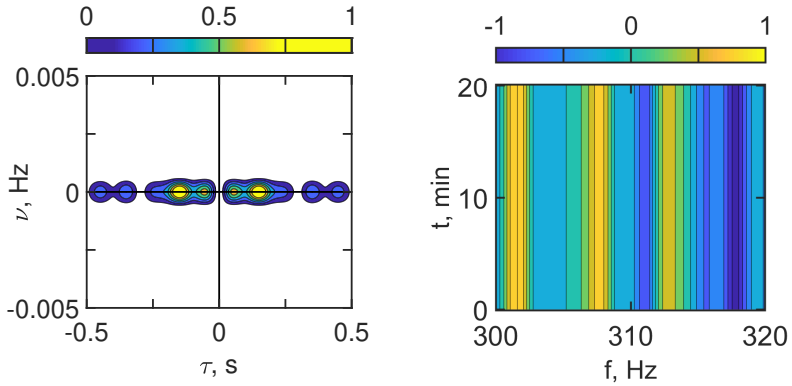

(a) (b)

Figure 9. Normalized filtered hologram $F(\tau, \widetilde{\nu})$ (**a**) and filtered interferogram $I(f, t)$ (**b**). Frequency range $\Delta f_2 = 300 - 320$ Hz. Non-moving source ($v = 0$ m/s). IIWs are present ($B_n = 15$ m, $u_n = 0.7$ m/s).

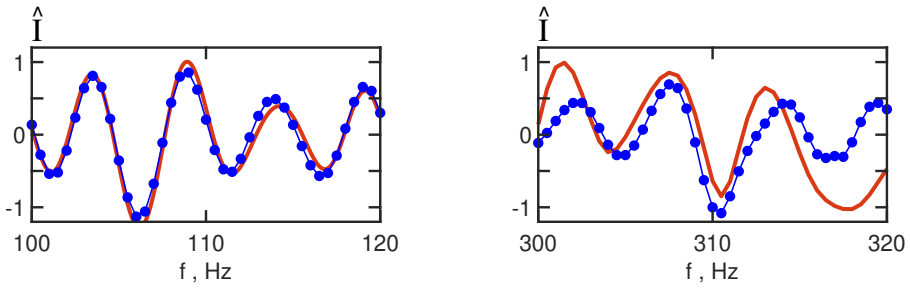

(a) (b)

Figure 10. Reconstructed 1D-interferogram $I(f)$ (**a**) $\Delta f_1 = 100 - 120$ Hz and (**b**) $\Delta f_2 = 300 - 320$ Hz. Non-moving source ($v = 0$ m/s). Red curve - IIWs are absent. Blue curve - IIWs are present.

The numerical modeling results for the frequency range $\Delta f_2 = 300 - 320$ Hz are identical to those for the range $\Delta f_1 = 100 - 120$ Hz. From the presented results it follows that the described method allows to separate the sound field component corresponding to the waveguide without IIWs and the sound field component related to the interference by IIWs. Thus, the interferogram of the waveguide without IIWs can be reconstructed for the case of the non-moving source in the presence of IIWs.

4.3. Moving source ($v = 1\,m/s$)

Let us consider the results of numerical modeling for a moving source ($v = 1\,m/s$). At the initial time $t_0 = 0$, the source-receiver range is $x_0 = 10\,km$. The source depth is $z_s = 20$ m. The receiver depth is $z_q = 45$ m. The source moves along the horizontal axis X to the receiver. The velocity of the source is $v = 1$ m/s. The source spectrum is uniform. The sound field pulses have duration $t_1 = 4\,s$ (sampling frequency 0.25 Hz). The interval between the end of the previous and the beginning of the next pulse $t_2 = 1$ s. So, time interval between pulses $t^* = 5$ s, ($t^* = t_1 + t_2$). The time observation is $\Delta t = 20$ min. The two frequency bands $\Delta f_1 = 100 - 120$ Hz (Table 1) and $\Delta f_2 = 300 - 320$ Hz (Table 2) are considered.

The results of the numerical modeling are shown in Figures 12–17. The dashed lines on the holograms show the band where the focal spots of the sound field of the moving source are concentrated in the waveguide without IIWs. It can be seen that the linear size of the band: $\delta\tau \approx 0.15$ s, $\delta\nu \approx 0.002$ Hz corresponds to the theoretical estimates of the focal spots sizes $\delta\tau = 0.1$ s, $\delta\nu = 0.0017$ Hz.

Figure 12 and Figure 13 show the interferogram $I(f,t)$ and the hologram $F(\tau,\widetilde{\nu})$ of the moving source for the case where there is no IIWs. The Figure 12 corresponds to $\Delta f_1 = 100 - 120$ Hz and Figure 13 to $\delta f_2 = 300 - 320$ Hz. The interferograms $I(f,t)$ consist of localized angled fringes. The hologram $F(\tau,\widetilde{\nu})$ consists of focal spots in the dotted line band. This is the result of the movement of the source. The irregularity of the interferogram $I(f,t)$ and the number of focal spots in the hologram $F(\tau,\widetilde{\nu})$ increase with frequency, as they do for a non-moving source.

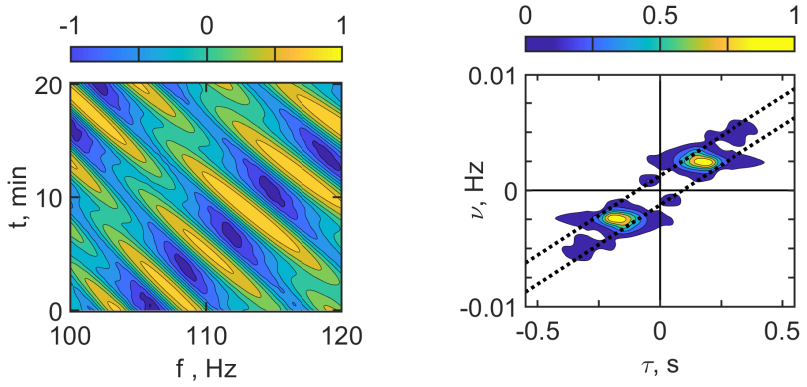

Figure 11. Normalized interferogram $I(f,t)$ (**a**) and hologram $F(\tau,\widetilde{\nu})$ (**b**). Frequency range $\Delta f_1 = 100 - 120$ Hz. Moving source ($v = 1$ m/s). IIWs are absent.

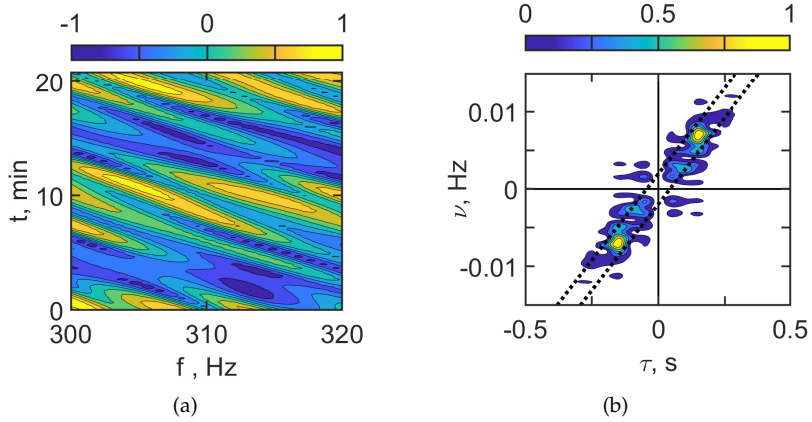

Figure 12. Normalized interferogram $I(f,t)$ (**a**) and hologram $F(\tau,\widetilde{\nu})$ (**b**). Frequency range $\Delta f_2 = 300 - 320$ Hz. Moving source ($v = 1$ m/s). IIWs are absent.

The estimates of the interferogram and hologram parameters:

1. $\Delta f_1 = 100 - 120$ Hz:
   interference fringes angular coefficients: $\delta f/\delta t \approx -0.015$ s^{-2},
   first focal spot coordinates $\tau_1 = 1.30 \cdot 10^{-1}$ s, $v_1 = 1.79 \cdot 10^{-3}$ Hz,
   source parameters (range and velocity): $\dot{v} = 1.0$ m/s, $\dot{x}_0 = 11.8$ km.
2. $\Delta f_2 = 300 - 320$ Hz:
   interference fringes angular coefficients: $\delta f/\delta t \approx -0.04$ s^{-2},
   first focal spot coordinates $\tau_1 = 4.08 \cdot 10^{-1}$ s, $v_1 = 1.54 \cdot 10^{-3}$ Hz,
   source parameters (range and velocity): $\dot{v} = 1.0$ m/s, $\dot{x}_0 = 12.0$ km.

Figures 14 and Figure 15 show the interferogram $I(f,t)$ and the hologram $F(\tau,\widetilde{\nu})$ of the moving source in the case of IIWs presence. Figure 14 corresponds to $\Delta f_1 = 100 - 120$ Hz and Figure 15 to $\Delta f_2 = 300 - 320$ Hz. When the acoustic track is located between the crests of the IS (horizontal spatial period $\Lambda = 250$ m), the interferogram $I(f,t)$ contains

horizontal fringes with the width $\Delta t = 5.8$ min. In this case, the sound field of the source is focused along the acoustic track due to the horizontal refraction caused by IIWs. Such a structure of the interferogram $I(f,t)$ with horizontal fringes leads to the formation of a periodic structure of focal spots in the hologram $F(\tau,\widetilde{\nu})$.

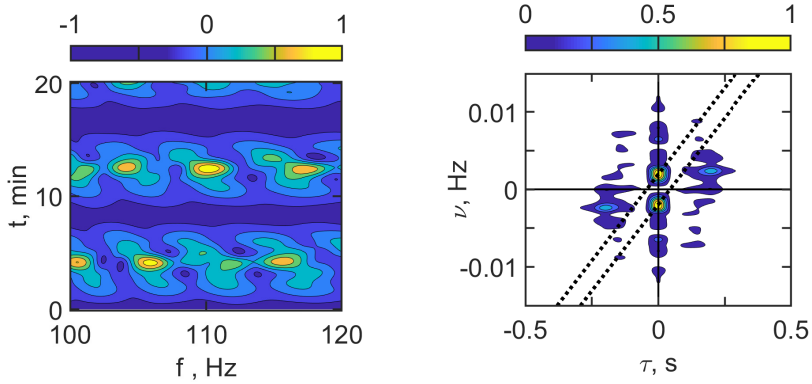

Figure 13. Normalized interferogram $I(f,t)$ (**a**) and hologram $F(\tau,\widetilde{\nu})$ (**b**). Frequency range $\Delta f_1 = 100 - 120$ Hz. Moving source ($v = 1$ m/s). IIWs are present ($B_n = 15$ m, $u_n = 0.7$ m/s).

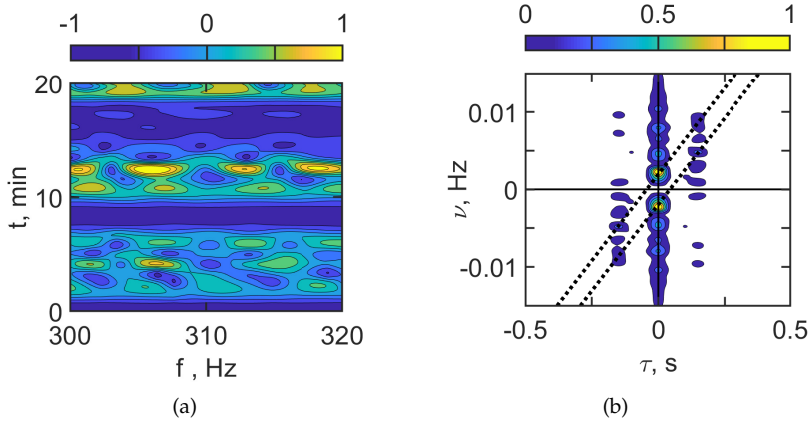

Figure 14. Normalized interferogram $I(f,t)$ (**a**) and hologram $F(\tau,\widetilde{\nu})$ (**b**). Frequency range $\Delta f_2 = 300 - 320$ Hz. Moving source ($v = 1$ m/s). IIWs are present ($B_n = 15\,\mathrm{m}$, $u_n = 0.7$ m/s).

The estimates for the focal spots sizes δf, δt, periodicity intervals L_f and L_t are as follows:

1. $\Delta f_1 = 100 - 120$ Hz;
   $\delta f_1 = 2.4$ Hz, $\delta t_1 = 1.1$ min;
   $L_{f_1} = 5.6$ Hz, $L_{t_1} = 8.3$ min.
2. $\Delta f_2 = 300 - 320$ Hz;
   $\delta f_2 = 2.8$ Hz, $\delta t_2 = 1.1$ min;
   $L_{f_2} = 6.8$ Hz, $L_{t_2} = 8.1$ min.

The structure of the arrangement of focal spots in the hologram $F(\tau,\widetilde{\nu})$ of the moving source allows to separate the sound field component corresponding to the waveguide without IIWs and the sound field component related to the disturbance by IIWs.

The results of the filtration of the hologram focal spots, shown in the dotted lines of Figure 14 and Figure 15 and their inverse 2D FT (interferogram) are shown in Figure 16 and Figure 17. The reconstructed interferograms and holograms in Figure 16 and Figure 17 correspond to the interferograms and holograms without IIWs in Figure 12 and Figure 13.

It can be seen that the focal spots on the reconstructed and the initial hologram are close to each other.

The estimates of the filtered interferogram and filtered hologram parameters read:

1. $\Delta f_1 = 100 - 120$ Hz:
   first focal spot coordinates $\tau_1 = 1.5 \cdot 10^{-1}$ s, $v_1 = 2.05 \cdot 10^{-3}$ Hz,
   source parameters (range and velocity): $\dot{v} = 1.2$ m/s, $\dot{x}_0 = 13.7$ km.
2. $\Delta f_2 = 300 - 320$ Hz:
   first focal spot coordinates $\tau_1 = 4.08 \cdot 10^{-1}$ s, $v_1 = 1.54 \cdot 10^{-3}$ Hz,
   source parameters (range and velocity): $\dot{v} = 1.0\,\mathrm{m/s}$, $\dot{x}_0 = 12.0$ km.

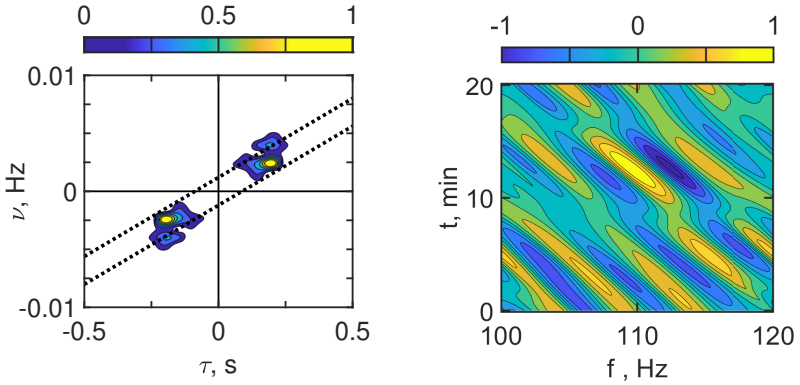

(a) (b)

Figure 15. Normalized filtered hologram $F(\tau, \widetilde{v})$ (**a**) and filtered interferogram $I(f, t)$ (**b**). Frequency range $\Delta f_1 = 100 - 120$ Hz. Moving source ($v = 1$ m/s). IIWs are present ($B_n = 15$ m, $u_n = 0.7$ m/s).

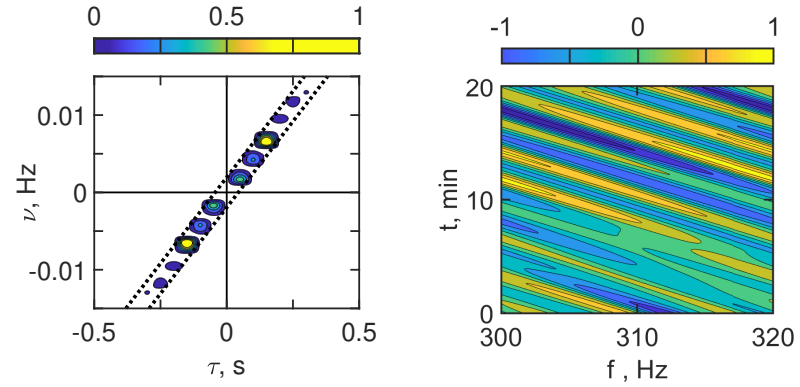

(a) (b)

Figure 16. Normalized filtered hologram $F(\tau, \widetilde{v})$ (**a**) and filtered interferogram $I(f, t)$ (**b**). Frequency range $\Delta f_2 = 300 - 320$ Hz. Moving source ($v = 1$ m/s). IIWs are present ($B_n = 15$ m, $u_n = 0.7$ m/s).

It can be seen that the focal spots on the reconstructed and initial holograms of the moving source are the same. The proximity of the initial and reconstructed interferograms of the moving source is shown in Figure 17. Figure 17 shows the 1D interferograms for $t_0 = 0$ min. Red curve - IIWs are not present. Blue curve - IIWs are present.

The error of the interferogram reconstruction is estimated by the dimensionless quantity Eq. (22):

1. $\Delta f_1 = 100 - 120$ Hz;
   $d_1 = 0.45$, $J = 80$.

2. $\Delta f_2 = 300 - 320$ Hz;
$d_2 = 0.60$, $J = 80$.

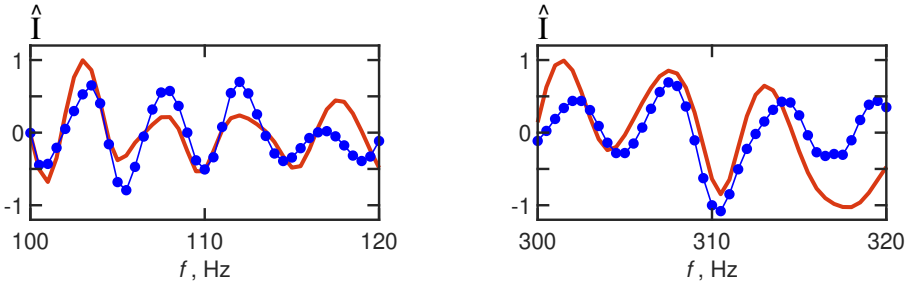

(a) (b)

Figure 17. Reconstructed 1D-interferogram $I(f)$ (**a**) $\Delta f_1 = 100 - 120$ Hz and (**b**) $\Delta f_2 = 300 - 320$ Hz. Moving source ($v = 1$ m/s). Red curve - IIWs are absent. Blue curve - IIWs are present.

Compared to the non-moving source, the error for the frequency ranges $\Delta f_1 = 100 - 120$ Hz and $\Delta f_2 = 300 - 320$ Hz has increased by a factor of 3.7 and 6.2, respectively. It can be seen that the interferogram of the waveguide without IIWs is reconstructed less accurately for the case of the moving source in the presence of IIWs. This difference in the error values is explained by the different situation of the variability of the propagation conditions. In the case of the non-moving source, there is a temporal variability of the waveguide only due to the IIWs. In the case of the moving source, there is a temporal variability of the waveguide due to IIWs and a spatio-temporal variability caused by the movement of the source.

5. Conclusions

In the framework of numerical simulation, we investigated the stability of the holographic signal processing method in the case of the moving broadband acoustic source source in the presence of IIWs. IIWs are assumed to propagate across the acoustic track (source-receiver). In this case, IIWs cause significant horizontal refraction of the sound field. As a result, the dynamic horizontal waveguides are approximately parallel to the IIW fronts in the horizontal plane.

The stability of holographic signal processing is based on the hologram structure of the moving source in the presence of IIWs. The hologram of the moving source consists of two disjoint components. The first is the sound field component corresponding to the waveguide without IIWs. The second component is the perturbation of the sound field by the IIWs causing horizontal refraction.

Such a hologram structure allows the separation of the sound field components. It is possible to filter the first component with minimal distortion. The filtered hologram component is used to reconstruct the interferogram of a moving source in the waveguide in the absence of IIWs. The reconstructed sound field interferograms in the presence of IIWs and the interferograms in the waveguide without IIWs differ in contrast. However, the angular coefficients of the interference fringes are the same.

Thus, in the presence of IIWs, it is possible to estimate the parameters of the source (range, velocity, direction, etc.) from the reconstructed sound field component. With an increase in the frequency range, the error in estimating the source parameters decreases.

Author Contributions: Supervision and project administration, M.E. and S.P.; conceptualization and methodology, V.K. and S.P.; software, S.T., P.R., and N.L.; validation, M.E. and V.K.; formal analysis, M.E. and S.P.; writing—original draft preparation, M.E. and S.P.; writing—review and editing, M.E. and S.P.; All authors have read and agreed to the published version of the manuscript.

Funding: This work was supported by grant from the Russian Science Foundation № 23-61-10024, https://rscf.ru/project/23-61-10024/.

Data Availability Statement: The data presented in this study are available on request from the corresponding author.

Conflicts of Interest: The authors declare no conflict of interest.

References

1. Harrison CH. The relation between the waveguide invariant, multipath impulse response, and ray cycles. *J. Acoust. Soc. Am., 129(5):2863-2877.* **2011**.
2. Kuperman WA, D'Spain GL. Ocean acoustic interference phenomena and signal processing. *Ocean Acoust. Interfer. Phenom. Signal Proc. 621* **2002**.
3. Rouseff D, Spindel RC. Modeling the waveguide invariant as a distribution. *AIP Conference Proceedings, American Institute of Physics 621:137-150.* **2002**.
4. Baggeroer AB. Estimation of the distribution of the interference invariant with seismic streamers. *AIP Conf. Proc., Amer. Inst. Phys. 621:151–170.* **2002**.
5. Yang T. Beam intensity striations and applications. *J. Acoust. Soc. Am., 113(3):1342-1352.* **2003**.
6. Heaney KD. Rapid geoacoustic characterization using a surface ship of opportunity. *IEEE J. Oceanic Engrg., 29(1):88-99.* **2004**.
7. Thode AM. Source ranging with minimal environmental information using a virtual receiver and waveguide invariant theory. *J. Acoust. Soc. Am., 108(4):1582-1594.* **2000**.
8. Cockrell KL, Schmidt H. Robust passive range estimation using the waveguide invariant. *J. Acoust. Soc. Am., 127(5):2780-2789.* **2010**.
9. Ianniello J. Recent developments in sonar signal processing. *IEEE Signal Proc. Magazine, 15(4):27-40.* **1998**.
10. Emmetiere R, Bonnel J, Gehant M, Cristol X, Chonavel Th. Understanding deep-water striation patterns and predicting the waveguide invariant as a distribution depending on range and depth. *J. Acoust. Soc. Am., 143(6):3444-3454.* **2018**.
11. Emmetiere R, Bonnel J, Cristol X, Gehant M, Chonavel T. Passive source depth discrimination in deep-water. *IEEE J. of Selected Topics in Signal Processing, 13(1):185-197.* **2019**.
12. Ehrhardt M, Pereselkov S, Kuz'kin V, Tkachenko S, Rybyanets P, Ladykin N. Use of Interference Patterns to Control Sound Field Focusing in Shallow Water. *J. Mar. Sci. Eng., 11(3):559.* **2023**.
13. Kuznetsov GN, Kuzkin VM, Pereselkov SA. Spectrogram and localization of a sound source in a shallow sea. *Acoust. Phys., 63(4):449-461.* **2017**.
14. Kaznacheev IV, Kuznetsov GN, Kuzkin VM, Pereselkov SA. Interferometric method for detecting a moving sound source with a vector-scalar receiver. *Acoust. Phys., 64(1):37-48.* **2018**.
15. Pereselkov SA, Kuz'kin VM. Interferometric processing of hydroacoustic signals for the purpose of source localization. *J. Acoust. Soc. Am., 151(2):666-676.* **2022**.
16. Ehrhardt M, Pereselkov SA, Kuz'kin VM, Kaznacheev I, Rybyanets P. Experimental observation and theoretical analysis of the low-frequency source interferogram and hologram in shallow water. *J. Sound Vibr. 544:117388.* **2023**.
17. Kaznacheev IV, Kuz'kin VM, Kutsov MV, Lyakhov GA, Pereselkov, SA. Interferometry in Acoustic-Data Processing Using Extended Antennas. Space-Time Analogy. *Phys. Wave Phenom., 28(4):326-332.* **2021**.
18. Kuz'kin VM, Matvienko YV, Pereselkov SA, Prosovetskii DY, Kaznacheeva ES. Mode selection in oceanic waveguides. *Phys. Wave Phenom., 30(2):111-118.* **2022**.
19. Kuz'kin VM, Pereselkov SA, Matvienko YV, Tkachenko SA. Detection of a Noise Signal in an Oceanic Waveguide Using a Vertical Array. *Phys. Wave Phenom., 29(4):323-329.* **2022**
20. Kaznacheeva ES, Kuz'kin VM, Lyakhov GA, Pereselkov SA, Tkachenko SA. Adaptive Algorithms for Interferometric Processing. *Phys. Wave Phenom., 28(3):267-273.* **2020**
21. Kuz'kin VM, Kuznetsov GN, Pereselkov SA, Grigor'ev VA. Resolving Power of the Interferometric Method of Source Localization. *Phys. Wave Phenom., 26(2):150-159.* **2018**
22. Kuz'kin VM, Pereselkov SA, Kuznetsov GN, Kaznacheev IV. Interferometric Direction Finding by a Vector-Scalar Receiver. *Phys. Wave Phenom., 26(1):63-73.* **2018**
23. Apel JR, Badiey M, Chiu C-S, Finette S, Headrick RH, Kemp J, Lynch JF, Newhall AE, Orr MH, Pasewark BH, Tielburger D, Turgut A, von der Heydt K, Wolf SN. An overview of the SWARM 1995 shallow-water internal wave acoustic scattering experiment. *IEEE J. Ocean. Engrg., 22:465-500.* **1997**.

24. Frank SD, Badiey M, Lynch J, Siegmann WL. Analysis and modeling of broadband airgun data influenced by nonlinear internal waves. *J. Acoust. Soc. Am., 116(6):3404-3422.* **2004**.
25. Badiey M, Katsnelson BG, Lynch JF, Pereselkov S, Siegmann WL. Measurement and modeling of three-dimensional sound intensity variations due to shallow-water internal waves. *J. Acoust. Soc. Am., 117(2):613-625.* **2005**.
26. Badiey M, Katsnelson BG, Lynch JF, Pereselkov S. Frequency dependence and intensity fluctuations due to shallow water internal waves. *J. Acoust. Soc. Am., 122(2):747-760.* **2007**.
27. Kuz'kin VM, Pereselkov SA, Zvyagin VG, Malykhin AYu, Prosovetskiy DYu. Intense internal waves and their manifestation in interference patters of received signals on oceanic shelf. *Phys. Wave Phenom., 26(2):160-167.* **2018**.
28. Badiey M, Kuz'kin VM, Lyakhov GA, Pereselkov SA, Prosovetskiy DYu,Tkachenko SA. Intense internal waves and their manifestation in the interference patterns of received signals on oceanic shelf. Part II. *Phys. Wave Phenom., 27(4):313-319.* **2019**.
29. Kaznacheeva ES, Kuz'kin VM, Pereselkov SA. Interferometric processing of hydroacoustic information in the presence of intense internal waves. *Phys. Wave Phenom., 29(3):278-284.* **2021**.
30. Kuzkin VM, Lyakhov GA, Pereselkov SA, Kaznacheeva ES. Transmission of information through a randomly inhomogeneous oceanic medium. *Fundam. Appl. Hydrof., 14(2):54-64.* **2021**.
31. Brekhovskikh LM, Lysanov YP. Fundamentals of Ocean Acoustics. *Springer.* **2013**.
32. Katsnelson BG, Pereselkov SA. Low-frequency horizontal acoustic refraction caused by internal wave solitons in a shallow sea. *Acoust. Phys., 46(6):684-691.* **2000**.
33. Katsnelson BG, Pereselkov SA. Space-Frequency Dependence of the Horizontal Structure of a Sound Field in the Presence of Intense Internal Waves. *Acoust. Phys., 50(2):169-176.* **2004**.
34. Konyaev KV, Sabinin KD. Waves inside the ocean. *St. Petersburg, Gidrometeoizdat Publ., 271 p.* **1992**.
35. Smith KB, Tappert FD. UMPE: The University of Miami Parabolic Equation Model. *Version 1.1 "MPL Technical Memorandum 432", P. 96.* **1993**.
36. Tappert FD. The parabolic approximation method. Lecture Notes in Physics, V. 70, Eds. J.B. Keller, J.S. Papadakis, Eds., Wave Propagation and Underwater Acoustics, *Springer-Verlag, New York, Chapter 5, pp. 224-287.* **1977**.
37. Zhou J, Zhang XZ, Rogers PH. Resonant interaction of sound wave with internal solitons in the coastal zone. *J. Acoust. Soc. Am., 90(4):2042-2054.* **1991**.
38. Silver AN. Manifestation of the properties of solitons in internal waves on the shelf. *Izv. Academy of Sciences of the USSR, Physics of the Atmosphere and Ocean, 29(2):285-293.* **1993**.
39. Hsu MK, Liu AK, Liu C. An study of internal waves in the China seas and yellow sea using SAR. *Contin. Shelf Res., 20(4-5):389-410.* **2000**.